Australian Government
Department of Defence
Defence Science and
Technology Organisation

Modelling of Thermal Line Scanning for the Inspection of Delamination in Composites and Cracking in Metals

N. Rajic

Air Vehicles Division
Platforms Sciences Laboratory

DSTO–TR–1673

ABSTRACT

This report describes a predictive capability, comprising analytical and numerical models, for the development and assessment of thermal line-scanning, an emerging non-destructive technique for the rapid inspection of aircraft structural components. The models describe the two-dimensional heat diffusion process pertaining to the application of a thermal line source to an object moving at constant velocity. Relevant case studies are considered including delamination in a composite laminate and cracking in a metal plate. Numerical experiments show that for planar flaws aligned with the inspection surface the performance of thermal line scanning is broadly equivalent to that of conventional flash thermography. In contrast, for a surface-breaking crack, where the flaw plane is typically perpendicular to the scan direction, strong lateral heat flows induced by a narrow beam provide a superior basis for inspection. For problems that involve distributed cracking, like in the wing carry-through bulkhead in the F/A-18 aircraft, the technique could offer an advantage over more conventional methods of inspection.

Published by

DSTO Platforms Sciences Laboratory
506 Lorimer St,
Fishermans Bend, Victoria, Australia 3207

Telephone: (03) 9626 7000
Facsimile: (03) 9626 7999

AR No. 013-316
December 2004

APPROVED FOR PUBLIC RELEASE

Modelling of Thermal Line Scanning for the Inspection of Delamination in Composites and Cracking in Metals

EXECUTIVE SUMMARY

The use of forced lateral heat-flow as a basis for detecting vertically-orientated surface flaws was canvassed in a rudimentary experimental study by DSTO researchers in 1998. As part of that investigation, an improvised point thermal-scanning non-destructive inspection facility was developed using a Helium-Neon laser source and a single element Cadmium-Mercury-Telluride detector. Attempts at detecting very small surface breaking cracks in metal coupons proved unsuccessful due to deficiencies in the improvised apparatus. However, the trials did provide some encouragement in that paint-layer thicknesses of the order of 10 microns were able to be systematically deduced from measurements of the phase shift in the response signal relative to an applied persistent harmonic excitation.

Although unsuccessful, the investigation fostered an ongoing interest in the principle of forced lateral diffusion, further strengthened by important prospective applications like, for example, the distributed cracking in the wing carry-through bulkhead in the F/A-18 aircraft. As a precursor to revisiting the earlier experimental program, equipped this time with improved hardware, it was thought instructive to first develop modelling tools that could assist in the design of an experimental facility and ultimately in the interpretation of experimental observations.

This report outlines the development and application of analytical and numerical models describing salient modes of heat diffusion in a line-scanning thermal inspection process. The models were applied to problems involving both in-plane and out-of-plane defect orientations. It was shown that when the direction of relative motion is largely parallel to the plane of the defect, the effects of a moving line source and a spatially uniform illumination are similar. That is, the flaw contrast is comparable in form and grows linearly with excitation intensity when the response is unforced. Whilst no advantage in performance could be ascribed to thermal line scanning in this situation, its adaptability to high-throughput inspection should not be overlooked as a practical benefit.

Superior performance was indicated for surface breaking cracks with a vertical orientation. The spatially uniform surface illumination characteristic of flash thermography invariably produces a co-aligned heat flow, rendering the technique ineffective for this type of problem. Numerical experiments have reinforced an expectation that lateral heat flows induced by a narrow line-source provide a far more effective basis for the detection of this critical form of damage.

More generally, the study reveals considerable scope for the design of tailored inspection regimes. Careful selection of scan velocity, with optimal design of the beam profile, should furnish markedly improved inspection outcomes. The models described in this report provide the requisite framework for such efforts.

Author

Nik Rajic
Airframes and Engines Division

Nik Rajic received a B. Eng. (Hons.) in Mechanical Engineering from the University of Melbourne in 1989. He joined Structures Division at the Aeronautical Research Laboratory in 1991 and in 1992 undertook studies at Monash University which led to the completion of a PhD in 1995. He has since contributed to research on fatigue-life extension techniques, thermoelastic stress analysis, thermoplasticity, thermographic nondestructive evaluation, and in situ structural health monitoring techniques based on smart structures principles. He is currently a Senior Research Scientist in the Air Vehicles Division.

Contents

Appendices

Figures

1 Introduction

The provision of structural integrity assurance for flight-critical aircraft structural components is a costly task, involving a regime of rigorous, usually labour-intensive, non-destructive inspection (NDI). This cost will invariably grow as designers pursue increased aircraft operational efficiency through more radical structural optimisation, a process that often leads to the creation of challenging inspection problems. Examples are not hard to find. The wing carry-through bulkhead on the F/A-18 aircraft, for instance, experiences high uniform stresses that are known to promote widespread fatigue cracking, an insidious form of damage where separate small flaws, each possibly innocuous and often undetectable, can rapidly coalesce leading to sudden and potentially catastrophic structural failure.

Challenging inspection problems like this stress the need for continued refinement and innovation in NDE technology. One such innovation is line scanning thermography (LST) (Maldague (1993)). Like its more established counterpart, flash thermography (FT), LST functions by inducing internal heat flows that interact with structural defects and other discontinuities to produce thermal contrasts. The notable difference is that instead of a spatially-uniform, or "sheet", illumination, LST employs a narrow line source that moves at constant velocity in relation to the subject, or vice versa, as illustrated in *Figure 1.* The key effect is that, along with heat flow induced in the surface-normal direction, temperature gradients are also established laterally in the plane of the inspection surface. When the dominant plane of a flaw is aligned perpendicular to the surface; quite typical of fatigue cracking; the advantage of lateral heat flow is clear. To flash thermography, and for that matter any technique involving energy-flow aligned in the surface-normal direction, such flaws are, in effect, transparent.

Another salient advantage is the adaptability of LST to high throughput inspection. This is especially relevant in a manufacturing environment, where inspections are typically repetitive and often require a large outlay in manual labour. Furthermore, installation of a LST capability in a production operation is likely to be straightforward given that existing infrastructure would normally satisfy the need for motion. In this sense, the technology has a considerable practical advantage over ultrasonic scanning facilities, which rely on good acoustic coupling and therefore require more conspicuous arrangements.

Notwithstanding the promise of the technique, its efficacy in relation to important aerospace applications is yet to be comprehensively assessed. In relying on processes of heat diffusion, LST is subject to some fundamental limitations, most notably a restricted penetration depth, which it shares with FT – in relation to which that issue has been thoroughly canvassed. However, some parameters; most notably scan velocity and line-source width; are unique to thermal line scanning and intuitively are expected to be instrumental factors in its performance, and yet have attracted relatively little consideration. An understanding of the role these factors play in the context of non-destructive inspection is vital to a proper assessment of the technique, and is best sought through appropriate mathematical models of the relevant heat diffusion process. This report outlines the formulation of analytical and numerical models germane to this objective, and then considers two case studies in some detail: (i) delamination in a composite panel and (ii) cracking in a metal plate.

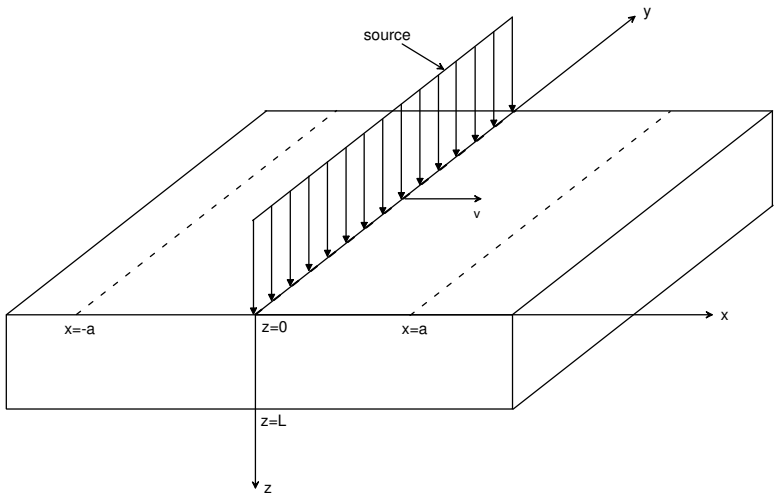

Figure 1: Schematic showing a slab of thickness L exposed to an infinitesimally thin line source originating at $x = -\infty$ and moving in the positive x direction at velocity v.

2 Analytical Models

The time-varying temperature distribution in a homogeneous plate is first described analytically. The result is later extended to handle an orthotropic material.

2.1 Homogeneous Plate

The Green's function for an infinite slab of thickness L with adiabatic boundary conditions is given by Carslaw and Jaeger (1984) as,

$$\tau = \frac{1}{8(\pi\kappa t)^{3/2}} e^{-\frac{(x-x')^2+(y-y')^2}{4\kappa t}} \sum_{n=-\infty}^{\infty} \{e^{-\frac{(2nl+z'-z)^2}{4\kappa t}} + e^{-\frac{(2nl-z'-z)^2}{4\kappa t}}\}, \tag{1}$$

where τ is the temperature at a point $\{x, y, z\}$ due to an instantaneous point source at $\{x', y', z'\}$ releasing heat at time $t = 0$, and κ is the thermal diffusivity. For most engineering materials absorption of incident radiation can be assumed to occur within an infinitesimally thin layer adjacent to the surface, such that $z' = 0$. Equation 1 becomes,

$$\tau = \frac{1}{4(\pi\kappa t)^{3/2}} e^{-\frac{(x-x')^2+(y-y')^2}{4\kappa t}} \sum_{n=-\infty}^{\infty} e^{-\frac{(2nl-z)^2}{4\kappa t}}. \tag{2}$$

The extension to a moving frame of reference is achieved by considering the change in temperature induced by the injection of heat at the fixed rate q across the interval dt', assuming the source moves at velocity v in the direction of positive x. This is expressed as,

$$d\tau = \frac{q dt'}{4\rho C(\pi\kappa(t-t'))^{3/2}} e^{-\frac{(x-v(t-t'))^2+y^2}{4\kappa(t-t')}} \sum_{n=-\infty}^{\infty} e^{-\frac{(2nl-z)^2}{4\kappa(t-t')}}, \tag{3}$$

where ρ is the mass density and C is the specific heat. The temperature at time t is then,

$$\tau = \frac{q}{4\rho C(\pi k)^{3/2}} \sum_{n=-\infty}^{\infty} \int_{t'=0}^{t} \frac{1}{(t-t')^{3/2}} e^{-\frac{(x-v(t-t'))^2+y^2+(2nl-z)^2}{4\kappa(t-t')}} \, dt'. \tag{4}$$

Letting $r^2 = x^2 + y^2$ and defining,

$$\xi = \frac{r}{2\sqrt{\kappa(t-t')}}, \tag{5}$$

enables the integral in *Equation 4* to be expressed in the more convenient form,

$$\frac{4}{\kappa^{1/2} r} e^{\frac{xv}{2\kappa}} \int_{\frac{r}{2\sqrt{kt}}}^{\infty} e^{-(\alpha^2\varepsilon^2 + \frac{\beta^2}{\xi^2})} d\xi, \tag{6}$$

where

$$\begin{aligned} \alpha^2 &= \frac{r^2 + (2nl-z)^2}{r^2}, \\ \beta^2 &= \frac{v^2 r^2}{16\kappa^2}. \end{aligned} \tag{7}$$

Its solution yields,

$$\frac{\sqrt{\pi}}{2\alpha} e^{-2\beta\alpha}, \tag{8}$$

which, reinserted into Equation 4, gives,

$$\frac{q}{2\pi\kappa\rho C} e^{\frac{xv}{2\kappa}} \sum_{n=-\infty}^{\infty} \frac{e^{-\frac{v}{2\kappa}\sqrt{r^2+(2nl-z)^2}}}{\sqrt{r^2+(2nl-z)^2}}. \tag{9}$$

A line source extending infinitely in the y direction is realised by integrating the kernel in *Equation 9*, i.e.,

$$\int_{y=-\infty}^{\infty} \frac{e^{-\eta\sqrt{\gamma^2+y'^2}}}{\sqrt{\gamma^2+y'^2}} \, dy', \tag{10}$$

where

$$\begin{aligned} \gamma &= \sqrt{x^2 + (2nl-z)^2}, \\ \eta &= \frac{v}{2\kappa}, \end{aligned} \tag{11}$$

which, after the relevant transformation reduces to;

$$2K_0(\gamma\eta), \tag{12}$$

where K_0 is the zeroth order Bessel function of the first kind. After reinserting the relevant terms, the final expression is,

$$\tau(x,z,t) = \frac{q}{\pi\rho C\kappa}\, e^{\frac{xv}{2\kappa}} \sum_{n=-\infty}^{\infty} K_0\left(\frac{v}{2\kappa}\sqrt{x^2+(2nl-z)^2}\right). \tag{13}$$

2.2 Orthotropic Plate

A broadly similar development is followed for an orthotropic material but it begins with a modified Green's function, the formulation of which is described in the Appendix. The Green's function is written here as,

$$\tau = \frac{A}{t^{3/2}} e^{\frac{-\gamma r^2}{t}} \sum_{n=-\infty}^{\infty} e^{-\frac{\gamma(2nl+z'-z)^2}{t}} + e^{-\frac{\gamma(2nl-z'-z)^2}{t}}, \tag{14}$$

where

$$\begin{aligned} A &= \frac{(\rho C)^{3/2}}{8\sqrt{\pi^3 k_x k_y k_z}}, \\ \gamma &= \frac{1}{4\kappa_z}, \\ r^2 &= \frac{(x-x')^2}{k_{xr}} + \frac{(y-y')^2}{k_{yr}}, \end{aligned} \tag{15}$$

and k_x, k_y and k_z are the thermal conductivities in the x, y and z directions respectively, and the subscript r denotes the ratio with respect to the z component. Given the prevalence of quasi-isotropic lay-ups in composite manufacture, the derivation is focused on that particular case, for which $k_y = k_x$. Accepting again the assumption of near-surface absorption, the function becomes,

$$\frac{2A}{t^{3/2}}\, e^{-\frac{\gamma r^2}{t}} \sum_{n=-\infty}^{\infty} e^{-\frac{\gamma(2nl-z)}{t}} \tag{16}$$

For brevity, the inclusion of motion is not detailed as it mirrors the implementation for the homogeneous case. Omitting the algebra, a line integral in the y-direction gives:

$$\tau(x,z,t) = \frac{q}{\pi\sqrt{k_x k_z}} e^{\frac{xv}{2\kappa_x}} \sum_{n=-\infty}^{\infty} K_0\left(\frac{v}{2\kappa_z k_{xr}}\sqrt{x^2+k_{xr}(2nl-z)^2}\right) \tag{17}$$

where, as noted in the appendix, k_{xr} is the ratio between in-plane and out-of-plane diffusivities. It can be verified that *Equation 13* is equivalent to the expression given by Winfree et al (2001) for a through-transmission scanning arrangement where the observation is taken at $z = L$.

3 Numerical Models

While analytical approaches can often yield elegant and compact descriptions of system behaviour they provide only a limited capacity to describe, in any useful detail at least, the complexity often found in real problems. The inclusion of a realistic structural defect, for example, is seldom possible. In this respect, numerical models are clearly superior.

The aim in this section is to present a computationally efficient numerical strategy for the modelling of a structure containing a flaw. To facilitate comparison with the closed-form solutions, variations in the $y-$direction are again assumed absent, leading to a spatially two-dimensional problem. The governing equation for heat diffusion is then,

$$k_x \frac{\partial^2 \tau}{\partial x^2} + k_z \frac{\partial^2 \tau}{\partial z^2} - \rho C \frac{\partial \tau}{\partial t} + \dot{Q} = 0, \tag{18}$$

where $\dot{Q}$ is a source term, whilst all boundaries are assumed adiabatic, viz.,

$$\frac{\partial \tau}{\partial n} = 0, \tag{19}$$

where n is the direction normal to the surface. *Equation 18* can be expressed in a variety of discrete forms, however for multi-dimensional problems where an unconditionally stable solution is sought, the Alternative Direction Implicit (ADI) approach has some appealing characteristics. It exhibits the same second order accuracy of the better known Crank Nicolson scheme (Ames (1977)) but tends to be computationally more efficient for spatially large problems. This is achieved by splitting the differential operator into its constituent dimensions, each then solved successively, thus avoiding the numerically expensive inversion of a large banded diagonal matrix characteristic of purely implicit schemes. The variant used in this study is that proposed by Samaarski and Andreev (1963), which is summarised as follows:

$$\begin{aligned} (I - \frac{\Delta t}{2} D_x)\{w\}' &= (D_x + D_z)\{\tau\}^n + \{S\}^n, \\ (I - \frac{\Delta t}{2} D_z)\{w\}'' &= \{w\}', \\ \{\tau\}^{n+1} &= \{\tau\}^n + \Delta t \{w\}'', \end{aligned} \tag{20}$$

where

$$D_x = \frac{\partial^2}{\partial x^2},$$

$$D_z \;=\; \frac{\partial^2}{\partial z^2}, \tag{21}$$

and w' and w'' are intermediate fields, I is the identity matrix, n is the time index and S is a source term. Applied to *Equation 18* the first intermediate step results in a tridiagonal system of equations,

$$\begin{pmatrix} b & c & 0 & & .. & & & & \\ & b & c & b & .. & & & & \\ & & & & .. & & & & \\ & & & & .. & b & c & b & \\ & & & & .. & & 0 & b & c \end{pmatrix} \cdot \begin{pmatrix} w'_1 \\ w'_2 \\ w'_3 \\ . \\ . \\ w'_{N-2} \\ w'_{N-1} \\ w'_N \end{pmatrix} = \begin{pmatrix} F_1 \\ F_2 \\ F_3 \\ . \\ . \\ F_{N-2} \\ F_{N-1} \\ F_N \end{pmatrix}, \tag{22}$$

where

$$\begin{aligned} b &= -\frac{\Delta t \kappa_x}{2\Delta x^2}, \\ c &= 1 + 2\frac{\Delta t \kappa_x}{2\Delta x^2}, \\ F_l &= \frac{\kappa_x}{\Delta x^2}(\tau^n_{i+1,j} - 2\tau^n_{i,j} + \tau^n_{i-1,j}) + \frac{\kappa_z}{\Delta z^2}(\tau^n_{i,j+1} - 2\tau^n_{i,j} + \tau^n_{i,j-1}) + \frac{\dot{Q}^n_{i,j}}{\rho C}, \end{aligned} \tag{23}$$

and $l \in \{i = 1 \ldots N, j = 1 \ldots M\}$. As remarked earlier, the tridiagonal structure facilitates a relatively expedient computation compared to the full matrix inversion required by the Crank Nicolson scheme. The next step in *Equation 20* generates a similar tridiagonal system except the matrix coefficients reflect the D_z operator and the forcing term comprises the intermediate field w' computed in the preceding step.

4 Numerical Experiments

4.1 Validation

Validation of the closed form and numerical solutions is pursued by tackling a representative problem. Consider a transversely isotropic panel 4.5 mm thick with principal diffusivities of $\kappa_x = 2\,\mathrm{mm^2 sec^{-1}}$ and $\kappa_z = 1\,\mathrm{mm^2\,sec^{-1}}$, scanned at a velocity of $2\,\mathrm{mm\,s^{-1}}$; parameters broadly appropriate to the inspection of a graphite-epoxy plate. The analysis focuses on a strip 100 mm in length, discretised in both spatial coordinates at a step size of 0.1 mm, amounting to a mesh size of $\{x, z :\ 1000 \times 45\}$.

The numerical solution was developed over 4000 time steps at increments of 10 msecs, leading to a total integration time of 40 seconds, a duration deemed sufficient for the establishment of a steady state response, as required for consistency with the closed form

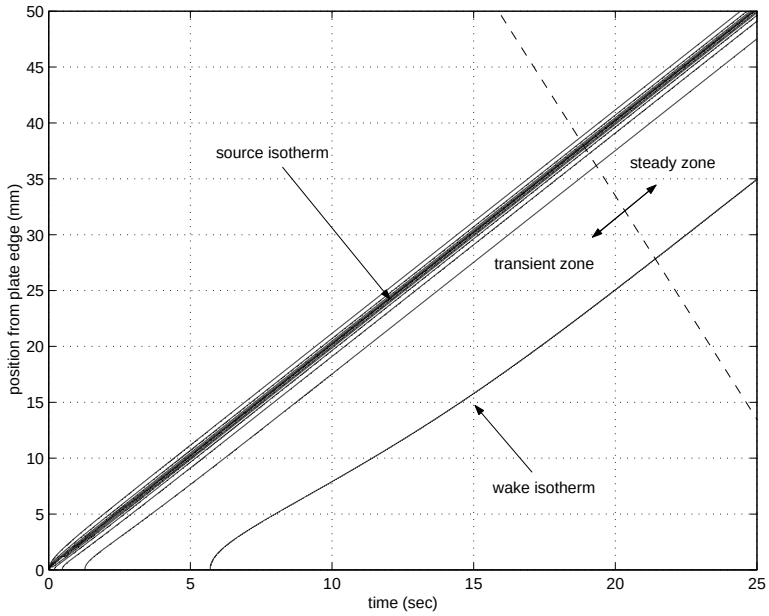

Figure 2: Development of source and wake isotherms for a source moving at constant velocity. Alignment of the isotherms occurs approximately 20 seconds after commencement.

solution. The attainment of a steady state is confirmed in *Figure 2* where a strong co-alignment is observed between the wake and source isotherms after a traversal length of about 30 mm. This is reinforced by the strong agreement between the solutions shown in *Figure 3*. A marginal discrepancy is noticeable in the wake of the source which is possibly caused by the inconsistency between the finite and infinite lateral domains assumed in the numerical and analytical formulations respectively.

4.1.1 Effect of Anisotropy

The effect of anisotropic material properties on the thermal response of polymer composite materials can be empirically discerned through a sensitivity analysis whereby the surface temperature evolution is computed for variations in the thermal diffusivity tensor. Analytical solutions were obtained for the case of a 5 mm thick graphite epoxy laminate with a thermal diffusivity of 2.8 $\text{mm}^2\,\text{s}^{-1}$ and 0.7 $\text{mm}^2\,\text{s}^{-1}$ in the x and z directions respectively (Plotnikov & Winfree (1998)), and at three scan velocities: 1, 10 and 100 $\text{mm}\,\text{s}^{-1}$. The comparison in *Figure 4* suggests that irrespective of velocity, the temperature decay in the wake of the source is far more rapid for the isotropic panel. This is readily explained by the reduced impediment to through-thickness heat flow relative to that of the composite panel, which also explains the consistently lower temperatures in advance of the source.

4.2 Planar Defects

We now consider an object containing a structural flaw, which for reasons already outlined, is a problem more effectively tackled using a numerical strategy. Two problems

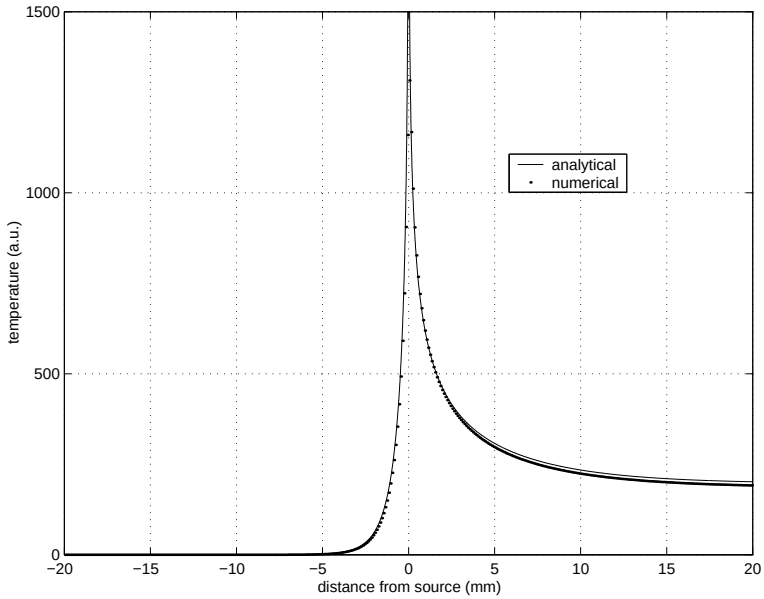

Figure 3: Model predictions for a $4.5\,\mathrm{mm}$ *thick transversely-isotropic panel with* $\kappa_\mathrm{x} = 2\ \mathrm{mm^2 sec^{-1}}$ *and* $\kappa_\mathrm{z} = 1\ \mathrm{mm^2 sec^{-1}}$*. Source traverses right to left in the figure.*

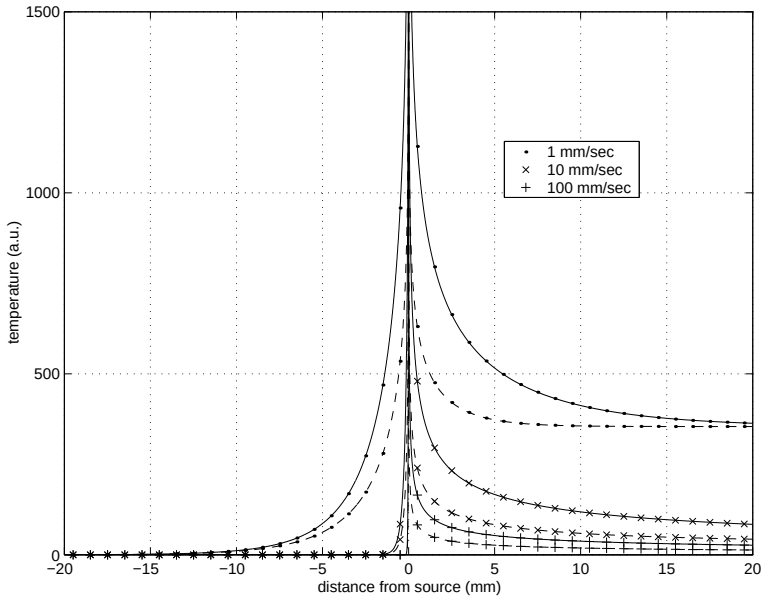

Figure 4: Steady temperature distribution in a $5\,\mathrm{mm}$ *thick plate for a line source at* $\mathrm{x} = 0$ *travelling from right to left. Dashed line corresponds to an isotropic plate:* $\kappa = 2.8\,\mathrm{mm^2 s^{-1}}$*, and the solid line to a transversely isotropic equivalent:* $\kappa_\mathrm{x} = \kappa_\mathrm{y} = 2.8\,\mathrm{mm^2 s^{-1}}$*,* $\kappa_\mathrm{z} = 0.7\,\mathrm{mm^2 s^{-1}}$*.*

are examined: (i) an in-plane delamination in a transversely isotropic composite laminate, and (ii) a small vertical crack in a metal plate.

It is seldom possible to develop a numerically simple representation of a flaw that does not in some manner involve an approximation. Instead, it is customary to conceive an approximate form, consistent with the numerical framework, that still captures the salient physical characteristics. In the context of thermal modelling, a first approximation is to assume a flaw is opaque to heat flow, and thus conceptually equivalent to a void with adiabatic surfaces. The approximation has obvious limitations. A kissing bond for instance will invariably admit some heat flow. An improvement in this case may be rendered with little increase in computational complexity by invoking the notion of an effective thermal resistance, which provides a convenient means of accommodating some measure of heat transfer across a flaw surface. However, the approach relies on a priori knowledge of the flaw structure, which is seldom available in practice. Regardless, for the broader objectives of this study, an adiabatic representation is sufficient and henceforth employed.

4.2.1 Composite Panel with Delamination

Recall the transversely isotropic panel described in *Figure 4*. A delamination is now introduced by inserting in the panel a void bounded by adiabatic surfaces. The void is 5 mm in length, equivalent to the panel thickness, and is inserted at a depth of 2.5 mm, precisely at the mid-plane. A line source is then applied at four scan velocities: 1, 10, 100 & 1000 $\mathrm{mm\,s^{-1}}$. The source is assumed to have a Gaussian spatial profile. This serves to best represent a true source, and also facilitates a simple means of ensuring a smooth lateral progression of the source across the discretised computational grid.

Figure 5 compares the computed contrast distributions. The intensity shown here is proportional to the metric $\theta = \tau - \tau_0$, where τ_o is the equivalent response of an unflawed panel. The signatures are qualitatively similar and differ most noticeably in the contrast intensity, which drops markedly with increased velocity. Moreover, inspection of the intensity scales reveals an apparently linear relationship between source velocity and peak contrast for some speeds, a characteristic shared with FT but with respect to pulse width. This suggests that a characteristic velocity might be defined that marks a transition whereby a line scanning event becomes, in its effect, equivalent to the application of a spatially uniform excitation.

The velocity at which the equivalence takes hold should be a function of the same parameters that control the timescale of any heat diffusion process, that is material thickness and thermal diffusivity. Raising a simple example to help clarify the point, a poor conductor with a deeply buried flaw is expected to exhibit a flash-type response at much lower velocities than a good conductor with a shallow flaw. In other words, thermal line scanning is expected to resemble a flash-type illumination when the source transit time is brief relative to the timescale of the transient response.

To underscore the similarity, evolutions of the contrast measured at a point centred above the delamination are presented in *Figure 6*. The timescale is referenced to the arrival of the source, so that negative times indicate an arriving source and positive times a departing one. It is evident that the contrast evolution approaches a constant form for velocities in excess of a certain value, in this case 5 mm/sec, which is reminiscent

of the type of behaviour anticipated for variations in pulse-width for a fixed sheet or flash-type illumination. Indeed, consider *Figure 7*, which shows the computed contrast evolutions for a spatially-uniform (sheet) excitation of varying duration. Here, a similar linear relationship is observed but as a function of pulse width, except for the last case, where an overlap between the transient response of the flaw and the excitation has caused a departure from linearity. A closer inspection (*Figure 8*) reveals evidence of departure at even shorter pulse widths, down to about one second. Using language synonymous with system dynamics, the response to an excitation in this case can be said to transform from free to forced as the pulse width exceeds this particular value.

An instructive and useful exercise is to relate the subject thermal diffusivity and a relevant length to a pulse width defining a transition from free to forced behaviour. To this end it is helpful to first invoke the concept of a thermal wave, the existence of which is most conveniently demonstrated by reducing the heat diffusion equation to its Helmholtz form. In the case of one-dimensional flow, the relevant expression is

$$\frac{d^2\hat{\tau}}{\partial z^2} = \frac{iw}{\kappa}\hat{\tau}, \tag{24}$$

where,

$$\tau = \hat{\tau}(z)\, e^{i(wt-\phi)}. \tag{25}$$

For a harmonic excitation of circular frequency w and arbitrary phase ϕ, i.e. $(\tau_o \sin(wt-\phi))$, applied at $z = 0$, the response can be expressed as,

$$\tau = \tau_o\, e^{-kz}\, \sin\left(wt - kz - \phi\right), \tag{26}$$

where k is the wavenumber,

$$k = \sqrt{\frac{w}{2\kappa}}, \tag{27}$$

which implies a thermal "wavelength" of,

$$\lambda = 2\sqrt{\frac{\kappa\pi}{f}}. \tag{28}$$

Note the exclusive dependence on thermal diffusivity and temporal frequency. It is also useful to note from *Equation 26* that diffusion is a highly attenuative process, viz., e^{-kz}, which suggests a reasonable approach, though admittedly somewhat arbitrary, is to assume a free response when $\lambda \leq L_z$, where L_z is an appropriate characteristic length, like the slab thickness or flaw depth. Simple arithmetic reveals an attenuation in excess of 50 dB at this length. Now reconsider, briefly, the case presented in *Figure 8*. Based on *Equation 28*, the pulse width satisfying this relation is approximately 400 msec, which accords well with the data shown in the figure.

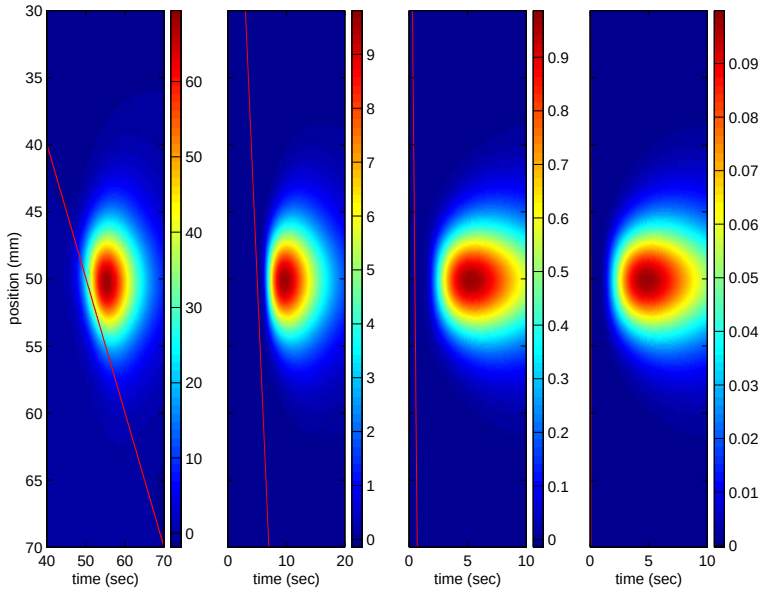

Figure 5: Contrast evolution computed for a 5 mm *thick composite panel with a* 5 mm *long adiabatic inclusion (synthetic delamination)* 2.5 mm *beneath the surface. Diagonal line traces source path. From left to right scan velocities are 1,10,100 & 1000* $\mathrm{mm\,sec^{-1}}$.

An adaptation to a line scanning configuration is straightforward. A second characteristic length is introduced to describe traversal of the source in the $x-$direction. Denoting this length L_x, *Equation 28* is rewritten to include a velocity term,

$$L_z \geq 2\sqrt{\frac{2\kappa\pi L_x}{v}} \tag{29}$$

In the absence of an appropriate specific length, the assignment $L_x = L_z$ is made, yielding,

$$v \geq \frac{8\kappa\pi}{L_z} \tag{30}$$

Revisiting the composite example, *Equation 30* yields a velocity of roughly $7\,\mathrm{mm\,s^{-1}}$, which again accords well with the relevant numerical data (*Figure 6*). Higher velocities manifest a largely free response.

4.2.2 Aluminium Panel with Subsurface and Surface Breaking Vertical Cracks

In the previous example it was shown that in applications where the flaw plane is aligned with the plane of the inspection surface the effect of a line source moving beyond a certain velocity is broadly equivalent to that of a uniform flash illumination. However, when the two planes in question are perpendicular, the equivalence no longer stands. In

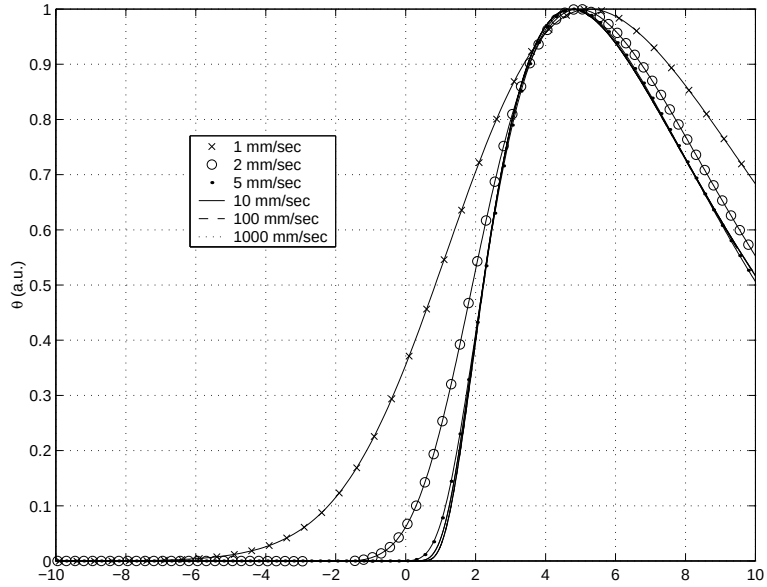

Figure 6: Normalised contrast evolution above centre of delamination for scan velocities of 1, 2, 5, 10, 100 & 1000 $\mathrm{mm\,sec^{-1}}$.

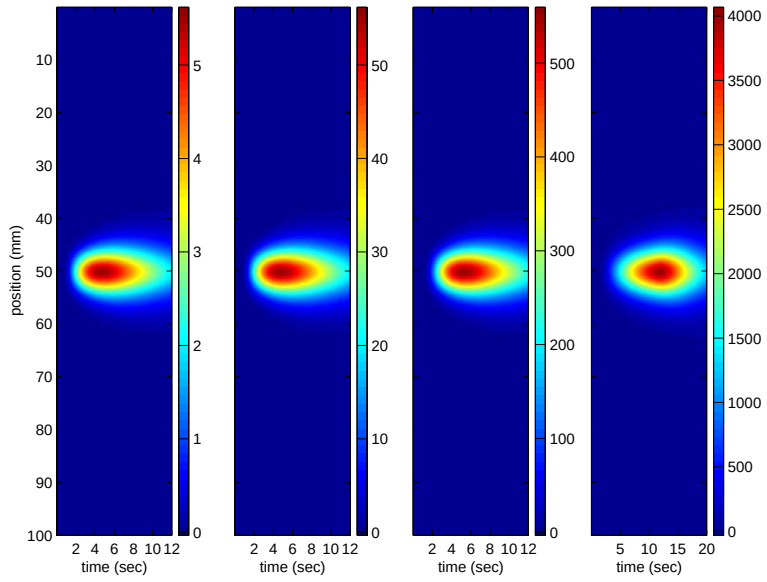

Figure 7: As in Figure 5 except for FT with pulse widths of 10, 100, 1000 and 10000 ms.

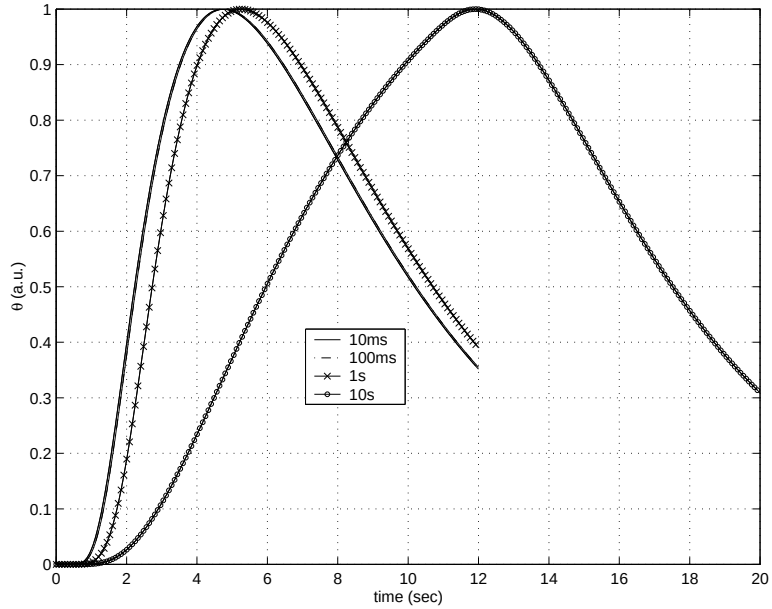

Figure 8: Normalised temperature contrast above centre of defect for pulse widths of 10, 100, 1000 & 10000 ms.

this situation FT is largely ineffective since the induced heat flow is aligned with, and consequently unimpeded by, the flaw. This is not the case with LST.

The problem of vertically orientated cracks has important practical significance in the context of military aircraft where weight and stress reduction imperatives have driven highly optimised designs that are susceptible to distributed cracking of this type. As remarked earlier, this is an insidious form of damage where crack coalescence can lead to rapid structural failure. It is useful therefore to consider the characteristic response of a vertical crack exposed to inspection by means of thermal line-scanning, and in particular to assess the effects on defect signature of key parameters like crack depth, source width, and scan velocity.

Two cracking problems are considered. Both involve the same basic geometry of a 5 mm thick aluminium alloy plate, 100 mm in length, containing in the first case a surface breaking (SB) crack of 0.5 mm in length and in the second a crack of identical length buried 2.5 mm beneath the plate surface. Analyses are performed for scan velocities of 1, 10 and 100 mm s^{-1}, both for an ideal narrow source profile and a broader variant (*Figure 9*). The effect of beam profile in the composite example considered earlier could be largely ignored on the basis of the low thermal diffusivity, the buried nature of the defect and its in-plane orientation. In this case however, lateral heat flow plays an instrumental role in fostering a strong indication. To this end, a sharp fall-off across the forward "edge" of the source is critical to sustaining a strong lateral gradient.

Figures 10–12 show computed surface contrast evolutions for the modelled SB crack. It affirms the anticipation of an elevated contrast on the source-side of the crack, mirrored on the shadow side by an inverted contrast. The highest contrast level apparently occurs on the source side just prior to the arrival of the source, however an exception in Figure 10 suggests this is not universally true and is likely a function of source profile and velocity

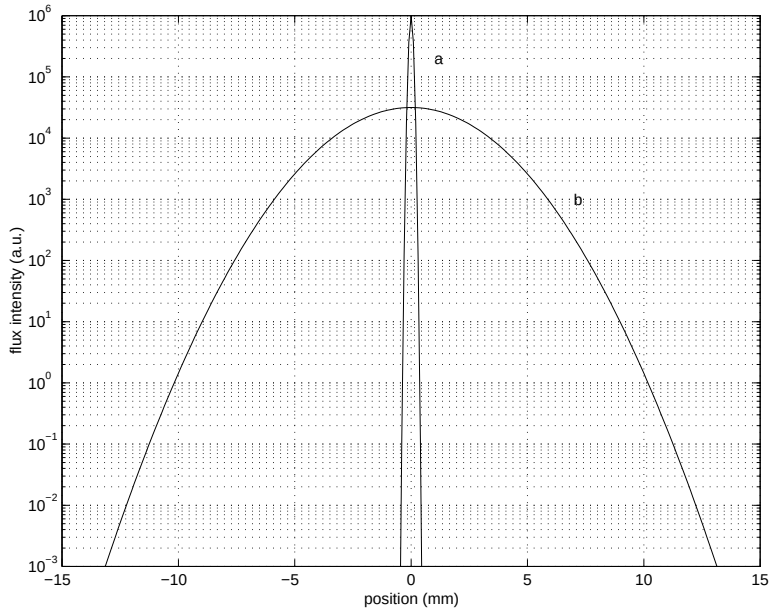

Figure 9: Different beam profiles with identical total radiant energy.

and, in all probability, also defect geometry. The effect of broadening the source profile is to cause both a temporal "smearing" of the contrast indication and a concomitantly weaker signal. In the absence of hardware constraints, for instance a slow image acquisition rate, a focused source would clearly prove more effective in practice for the inspection of these types of cracks.

The benefit of a spatially coherent source is not as significant when the crack is buried. In contrast to the previous example *Figures 13–15* indicate broadly similar contrast levels for the two beam profiles, with only a marginal advantage to the narrower variant. It is interesting to note that the form of the contrast evolution differs markedly from that of a SB crack, with evidently less anticipation of the source, which is due to the added diffusion length corresponding to the submerged depth. In this sense, the case bears some resemblance to the composite example considered earlier. For the buried crack, the peak intensity occurs later relative to the arrival of the source and is also noticeably weaker. This stems again from the added diffusion length and is an intuitive result.

5 CONCLUSION

A computational framework has been developed to provide a basis for predicting the performance of line-scanning thermography in the detection of planar and vertically orientated structural flaws. It was shown that the effect of line-scan excitation applied to a composite laminate is broadly equivalent to that of a flash inspection regime in the sense that the flaw contrast is similar in form and grows linearly with excitation intensity whilst the response remains unforced. Whilst no advantage in performance could be ascribed to thermal line scanning in this situation, its adaptability to high-throughput inspection should not be overlooked as a potential benefit.

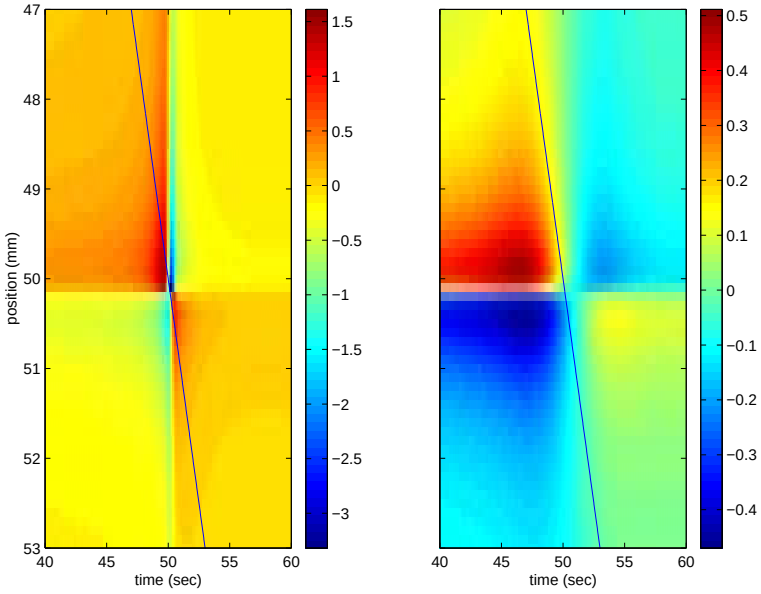

Figure 10: Contrast evolution computed for a 5 mm *thick Aluminium plate with a* 0.5 mm *deep surface-breaking crack. Diagonal line traces path of source. Source velocity* 1 $\mathrm{mm\,sec^{-1}}$

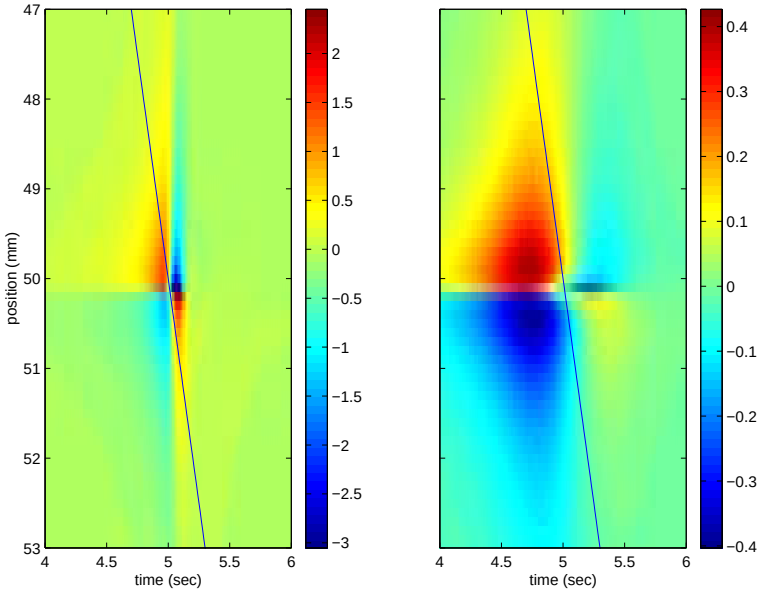

Figure 11: As above except source velocity 10 $\mathrm{mm\,sec^{-1}}$.

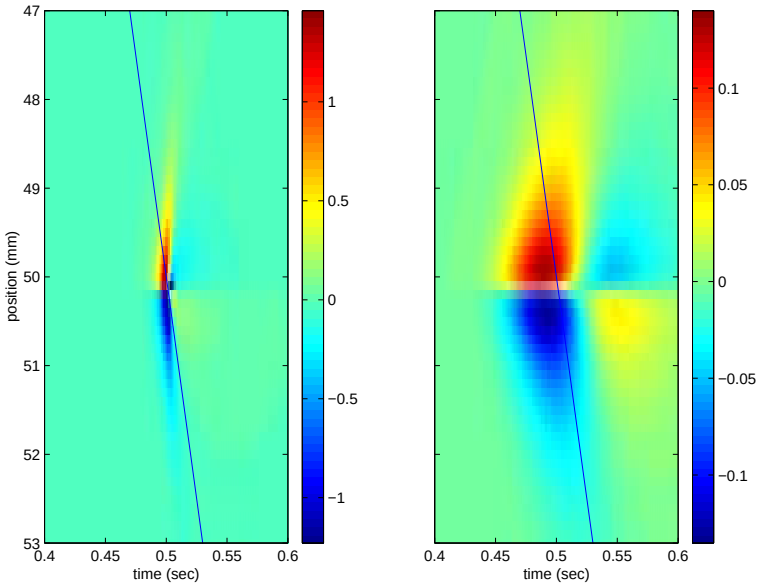

Figure 12: As above except source velocity 100 mm sec^{-1}.

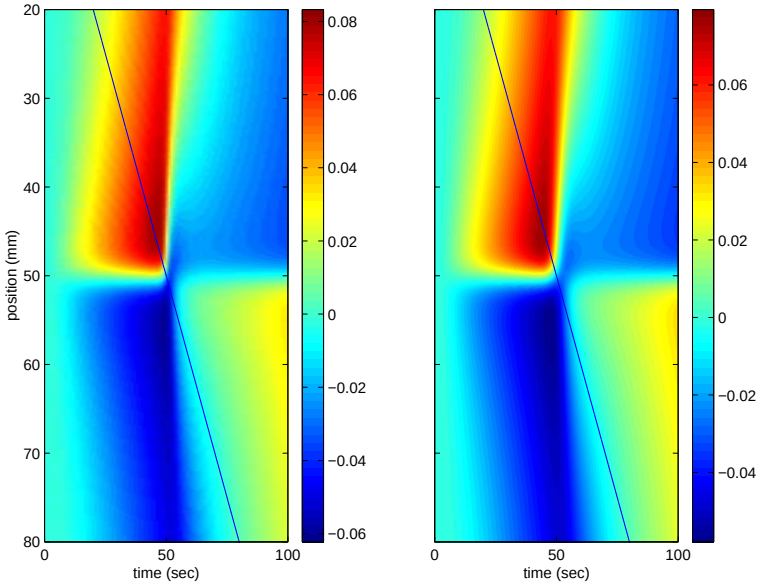

Figure 13: Contrast evolution computed for a 5 mm *thick Aluminium plate with a subsurface crack* 0.5 mm *in length extending downward from a depth of* 2.5 mm. *Diagonal line traces path of source. Source velocity* 1 mm sec^{-1}

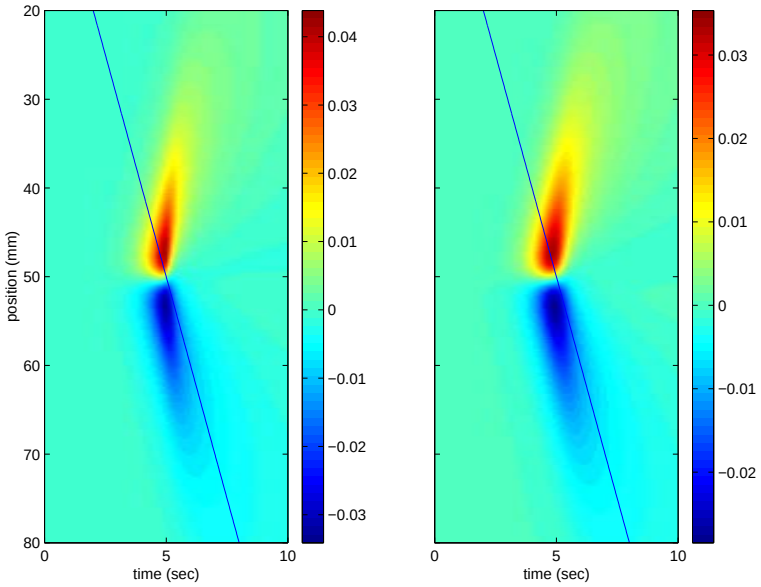

Figure 14: As above except source velocity 10 $\mathrm{mm\,sec^{-1}}$.

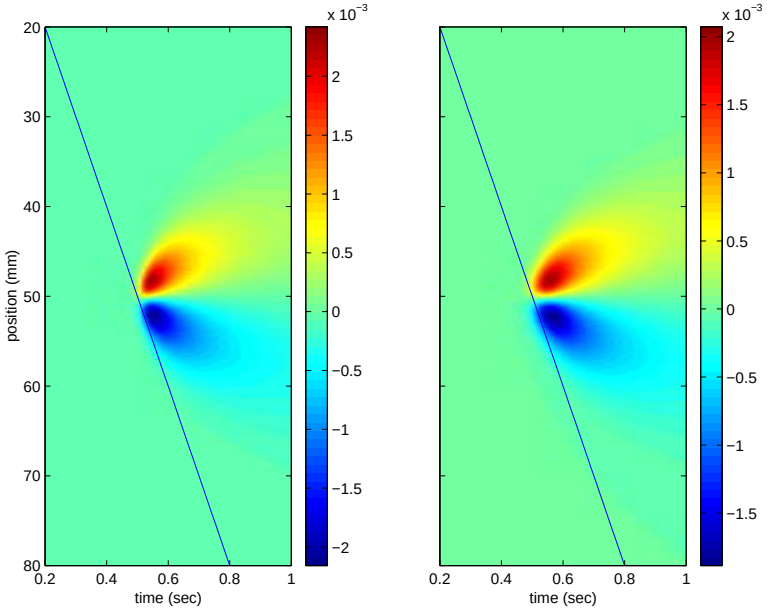

Figure 15: As above except source velocity 100 $\mathrm{mm\,sec^{-1}}$.

Superior performance was however indicated for surface breaking cracks with a vertical orientation. The spatially uniform surface illumination characteristic of flash thermography invariably leads to a co-aligned heat flow, rendering the technique ineffective for this type of problem. Numerical experiments have reinforced expectations that lateral heat flows induced by a narrow line-source provide a far more effective basis for the detection of this critically important form of fatigue damage. A submerged crack however mitigates the benefit of lateral flow, with a far weaker contrast expected for the same inspection regime.

More generally, the study reveals considerable scope for the design of tailored inspection regimes. Careful selection of scan velocity, with optimal design of the beam profile, should furnish markedly improved inspection outcomes. The models described in this report provide the requisite framework for such efforts.

Appendix A Green's Function for an Orthotropic Plate

The Greens function for an infinite plate with adiabatic surfaces can be conveniently obtained by considering first the expression for an infinite body,

$$\tau = \frac{(\rho C)^{3/2}}{8\sqrt{(\pi^3 t^3 k_x k_y k_z)}} e^{-\frac{\rho C}{4t}\left(\frac{(x-x'^2)}{k_x}+\frac{(y-y')^2}{k_y}+\frac{(z-z')^2}{k_z}\right)} \tag{A1}$$

Assuming linear heat flow, an adiabatic surface is introduced by using the principle of superposition. The source is simply mirrored outside the adiabatic surface creating a plane of symmetry. Since a plate requires two such surfaces, the source is mirrored in both directions, with each new source in turn mirrored with respect to the opposing surface to maintain the required symmetry. This is repeated indefinitely leading to an infinite sum in the expression,

$$\tau = \frac{(\rho C)^{3/2}}{8\sqrt{\pi^3 t^3 k_x k_y k_z}} e^{-\frac{\rho C r^2}{4k_z t}} \sum_{n=-\infty}^{\infty} e^{-\frac{\rho C(2nl+z'-z)^2}{4k_z t}} + e^{-\frac{\rho C(2nl-z'-z)^2}{4k_z t}} \tag{A2}$$

where

$$\begin{aligned} r^2 &= \frac{(x-x')^2}{k_{xr}} + \frac{(y-y')^2}{k_{yr}} \\ k_{xr} &= \frac{k_x}{k_z} \\ k_{yr} &= \frac{k_y}{k_z} \end{aligned} \tag{A3}$$

References

1. Ames, W. F., (1977), "Numerical Methods for Partial Differential Equations",*Academic Press, New York.*

2. Carslaw, H. S. and Jaeger, J. C., (1959), "Conduction of Heat in Solids",*Oxford University Press, Oxford.*

3. Maldague, X., (1993), "Nondestructive Evaluation of Materials by Infrared Thermography", *Springer-Verlag, London.*

4. Plotnikov, Y. A., and Winfree, W. P., (1998), "Thermographic Imaging of Defects in Ansiotropic Composites", *Review of Progress in QNDE*, **17A**, pp. 457–464.

5. Samarskii, A. A. and Andreev, V. B., (1963), "On a High Accuracy Difference Scheme for an Elliptical Equation with Several Space Variables",*U.S.S.R Comp. Math. Math. Phys.*, **3**, pp. 1373–1382.

6. Winfree, W. P., Heath, D. M., and Cramer, K. E., (2001), "Thermal Diffusivity Imaging with a Moving Line Source", *Thermosense XXIII, Andres E. Rozolnik, Ralph B. Dinwiddie, Editors, Proceedings of SPIE*, **4360**, pp. 606–615.

DISTRIBUTION LIST

Modelling of Thermal Line Scanning for the Inspection of Delamination in Composites and Cracking in Metals

N. Rajic

	Number of Copies
DEFENCE ORGANISATION	
Task Sponsor	
DPSL	1
S&T Program	
Chief Defence Scientist	1
FAS Science Policy	
AS Science Corporate Management	
Director General Science Policy Development	
Counsellor, Defence Science, London	Doc Data Sheet
Counsellor, Defence Science, Washington	Doc Data Sheet
Scientific Adviser to MRDC, Thailand	Doc Data Sheet
Scientific Adviser Joint	1
Navy Scientific Adviser	Doc Data Sheet and Dist List
Scientific Adviser, Army	Doc Data Sheet and Dist List
Air Force Scientific Adviser	Doc Data Sheet and Exec Summ
Scientific Adviser to the DMO M&A	Doc Data Sheet and Dist List
Scientific Adviser to the DMO ELL	Doc Data Sheet and Dist List
Platform Sciences Laboratory	
RLAM, Air Vehicles Division	1
RLSI, Air Vehicles Division	1
Nik Rajic	5
Steve Galea	1
Kelly Tsoi	1
David Rowlands	1
Steve Lamb	1
DSTO Library and Archives	
Library, Fishermans Bend	Doc Data Sheet
Library, Edinburgh	1 and Doc Data Sheet

Library, Sydney	Doc Data Sheet
Library, Stirling	Doc Data Sheet
Library, Canberra	Doc Data Sheet
Defence Archives	1
Capability Development Group	
Director General Maritime Development	Doc Data Sheet
Director General Capability and Plans	Doc Data Sheet
Assistant Secretary Investment Analysis	Doc Data Sheet
Director Capability Plans and Programming	Doc Data Sheet
Director Trials	Doc Data Sheet
Chief Information Officer Group	
Deputy Chief Information Officer	Doc Data Sheet
Director General Information Policy and Plans	Doc Data Sheet
AS Information Strategy and Futures	Doc Data Sheet
AS Information Architecture and Management	Doc Data Sheet
Director General Australian Defence Simulation Office	Doc Data Sheet
Director General Information Services	Doc Data Sheet
Strategy Group	
Director General Military Strategy	Doc Data Sheet
Director General Preparedness	Doc Data Sheet
Assistant Secretary Strategic Policy	Doc Data Sheet
Assistant Secretary Governance and Counter-Proliferation	Doc Data Sheet
Navy	
SO (SCIENCE), COMAUSNAVSURFGRP, NSW	Doc Data Sheet and Dist List
Director General Navy Capability, Performance and Plans, Navy Headquarters	Doc Data Sheet
Director General Navy Strategic Policy and Futures, Navy Headquarters	Doc Data Sheet
Deputy Director (Operations) Maritime Operational Analysis Centre, Building 89/90, Garden Island, Sydney Deputy Director (Analysis) Maritime Operational Analysis Centre, Building 89/90, Garden Island, Sydney	Doc Data Sheet and Dist List
Army	
ABCA National Standardisation Officer, Land Warfare Development Sector, Puckapunyal	Doc Data Sheet (pdf format)
SO (Science), Deployable Joint Force Headquarters (DJFHQ)(L), Enoggera QLD	Doc Data Sheet

SO (Science), Land Headquarters (LHQ), Victoria Barracks, NSW	Doc Data Sheet and Exec Summ
Air Force	
SO (Science), Headquarters Air Combat Group, RAAF Base, Williamtown	Doc Data Sheet and Exec Summ
Joint Operations Command	
Director General Joint Operations	Doc Data Sheet
Chief of Staff Headquarters Joint Operation Command	Doc Data Sheet
Commandant ADF Warfare Centre	Doc Data Sheet
Director General Strategic Logistics	Doc Data Sheet
Intelligence and Security Group	
DGSTA, Defence Intelligence Organisation	1
Manager, Information Centre, Defence Intelligence Organisation	1 (pdf format)
Assistant Secretary Capability Provisioning	Doc Data Sheet
Assistant Secretary Capability and Systems	Doc Data Sheet
Assistant Secretary Corporate, Defence Imagery and Geospatial Organisation	Doc Data Sheet
Defence Libraries	
Library Manager, DLS-Canberra	Doc Data Sheet
Library Manager, DLS-Sydney West	Doc Data Sheet
UNIVERSITIES AND COLLEGES	
Australian Defence Force Academy Library	1
Head of Aerospace and Mechanical Engineering, ADFA	1
Deakin University Library, Serials Section (M List), Geelong, Vic	1
Hargrave Library, Monash University	Doc Data Sheet
Librarian, Flinders University	1
OTHER ORGANISATIONS	
National Library of Australia	1
NASA (Canberra)	1
Serials Librarian, State Library of South Australia	1
INTERNATIONAL DEFENCE INFORMATION CENTRES	
US - Defense Technical Information Center	2
UK - Dstl Knowledge Services	2
Canada - Defence Research Directorate R&D Knowledge and Information Management (DRDKIM)	1

NZ - Defence Information Centre	1

ABSTRACTING AND INFORMATION ORGANISATIONS

Library, Chemical Abstracts Reference Service	1
Engineering Societies Library, US	1
Materials Information, Cambridge Scientific Abstracts,US	1
Documents Librarian, The Center for Research Libraries, US	1

SPARES

DSTO Edinburgh Library	5

Total number of copies:	41

DEFENCE SCIENCE AND TECHNOLOGY ORGANISATION DOCUMENT CONTROL DATA	1. CAVEAT/PRIVACY MARKING

2. TITLE	3. SECURITY CLASSIFICATION
Modelling of Thermal Line Scanning for the Inspection of Delamination in Composites and Cracking in Metals	Document (U) Title (U) Abstract (U)
4. AUTHOR	5. CORPORATE AUTHOR
N. Rajic	Platforms Sciences Laboratory 506 Lorimer St, Fishermans Bend, Victoria, Australia 3207

6a. DSTO NUMBER	6b. AR NUMBER	6c. TYPE OF REPORT	7. DOCUMENT DATE
DSTO–TR–1673	013-316	Technical Report	December 2004

8. FILE NUMBER	9. TASK NUMBER	10. SPONSOR	11. No OF PAGES	12. No OF REFS
2004/1052934/1	LRR 03/057	DPSL	20	6

13. URL OF ELECTRONIC VERSION	14. RELEASE AUTHORITY
http://www.dsto.defence.gov.au/corporate/reports/DSTO–TR–1673.pdf	Chief, Air Vehicles Division

15. SECONDARY RELEASE STATEMENT OF THIS DOCUMENT

Approved For Public Release

OVERSEAS ENQUIRIES OUTSIDE STATED LIMITATIONS SHOULD BE REFERRED THROUGH DOCUMENT EXCHANGE, PO BOX 1500, EDINBURGH, SOUTH AUSTRALIA 5111

16. DELIBERATE ANNOUNCEMENT

No Limitations

17. CITATION IN OTHER DOCUMENTS

No Limitations

18. DEFTEST DESCRIPTORS

Line scanning, Composite materials, Metals, Cracking (fracturing), Thermal Analysis

19. ABSTRACT

This report describes a predictive capability, comprising analytical and numerical models, for the development and assessment of thermal line-scanning, an emerging non-destructive technique for the rapid inspection of aircraft structural components. The models describe the two-dimensional heat diffusion process pertaining to the application of a thermal line source to an object moving at constant velocity. Relevant case studies are considered including delamination in a composite laminate and cracking in a metal plate. Numerical experiments show that for planar flaws aligned with the inspection surface the performance of thermal line scanning is broadly equivalent to that of conventional flash thermography. In contrast, for a surface-breaking crack, where the flaw plane is typically perpendicular to the scan direction, strong lateral heat flows induced by a narrow beam provide a superior basis for inspection. For problems that involve distributed cracking, like in the wing carry-through bulkhead in the F/A-18 aircraft, the technique could offer an advantage over more conventional methods of inspection.